SCIENTIFIC REPORTS

OPEN

Structural-Controlled Synthesis of Highly Efficient Visible Light TiO$_2$ Photocatalyst via One-Step Single-Mode Microwave Assisted Reaction

Kunihiko Kato, Yunzi Xin & Takashi Shirai

TiO$_2$ with different chemical structures are successfully synthesized via a one-step single-mode magnetic microwave (SMMW) assisted process, during where Ti selectively oxidizes in magnetic field under Ar-O$_2$ mixed atmosphere. The chemical state and band structure of the as-prepared TiO$_2$ are well-controlled by changing the volume fraction of O$_2$ (φO$_2$) during SMMW synthesis. Ti^{3+} self-doped TiO$_2$ (TiO$_{2-x}$, $0 < x < 2$) is synthesized under lower φO$_2$, while TiO$_2$ with specific core/shell structure (TiO$_{2+y}$ core/TiO$_{2-x}$-TiO$_{2+z}$ shell) is observed under higher φO$_2$. The as-synthesized TiO$_2$ with controlled structures show sufficient light absorption in visible region and quite narrow bandgap (2.05 eV$\sim$), whose value can be also tuned by φO$_2$ during SMMW synthesis. In addition, the synthesized TiO$_2$ exhibits highly efficient photocatalytic performance towards the degradation of Rhodamine B under UV and visible light irradiation. The formation mechanism for different structural TiO$_2$ can be attributed to the specific rapid heating and cooling dynamics induced by SMMW irradiation.

TiO$_2$ photocatalysis have been widely utilized due to its physical and chemical stability, high photocatalytic activity, and nontoxicity[1,2]. However, the wide bandgap (3.0–3.2 eV) of TiO$_2$ seriously limits its absorption wavelength and photocatalytic performance only in UV light region. Numerous efforts have been paid for enhancing photocatalytic performance of TiO$_2$ in visible light region by inducing doped level from metals[3,4] or nonmetals[5–8]. However, the element doping may cause thermal or crystal instability and an increase on carrier trapping, which may decrease the photocatalytic efficiency[9]. In recent years, Ti^{3+} self-doped TiO$_2$ has attracted much interest, since surface energy level induced by Ti^{3+} and oxygen vacancies can improve visible-light absorption and results in high photocatalytic performance[10–15].

In our previous paper, we initially reported a novel single-mode magnetic microwave (SMMW) assisted one-step synthesis of Ti^{3+} self-doped TiO$_2$[16]. Upon the one-step irradiation of SMMW in pure oxygen atmosphere, Ti target oxidizes in tens of second reaction by rapid temperature change. Such specific heating process can be attributed to the drastic change of MW absorbing property accompanied with changes of chemical state in obtained material. Here in the present research, TiO$_2$ with well-controlled chemical states and band structures were selectively prepared by altering the oxygen fraction (φO$_2$) in an Ar-O$_2$ mixed atmosphere during SMMW synthesis. Ti^{3+} self-doped TiO$_2$ (TiO$_{2-x}$, $0 < x < 2$) is synthesized under lower φO$_2$, while TiO$_2$ with specific core/shell (TiO$_{2+y}$ core/TiO$_{2-x}$-TiO$_{2+z}$ shell) structure is observed under higher φO$_2$. The structure-controlled TiO$_2$ show sufficient light absorption in visible region with narrower bandgap (2.05 eV$\sim$), whose value can be also well tuned by φO$_2$. Meanwhile, the synthesized TiO$_2$ show superior photocatalytic performance to commercial TiO$_2$ in degradation of Rhodamine B (RhB) under both UV and visible light irradiation. The formation mechanism for different structural TiO$_2$ is clarified based on systemically investigation on crystallinity analysis with X-ray diffraction (XRD) patter and Raman spectroscopy, confirmation of chemical state by X-ray photoelectric spectroscopy (XPS), characterization of electrical band structures with UV-visible and photoluminescence (PL) spectroscopy. The SMMW assisted synthesis process described in this paper provides new strategy for the development of functional metal oxides with well-controlled chemical structures and specific properties.

Advanced Ceramics Research Center, Nagoya Institute of Technology, Gokiso-cho, Showa-ku, Nagoya, Aichi, 466-8555, Japan. Correspondence and requests for materials should be addressed to T.S. (email: shirai@nitech.ac.jp)
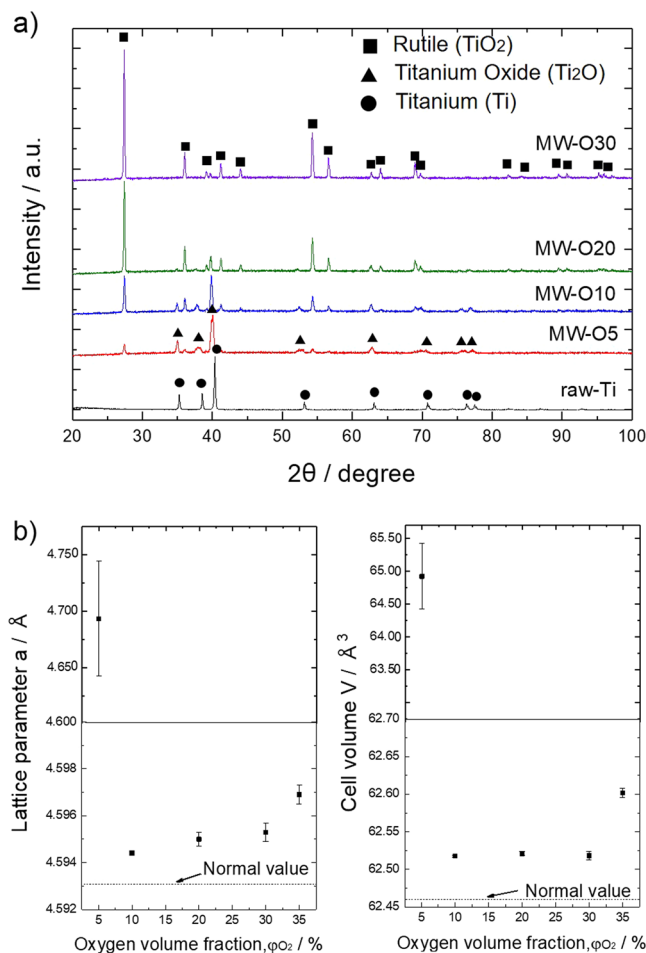
Figure 1. (**a**) XRD patterns of raw-Ti and as-prepared TiO_2. (**b**) Changes of the a-axis and cell volume of rutile TiO_2 synthesized under various atmosphere; the dashed lines indicate the value of rutile TiO_2 phase (JCPDS-ICDD card No. 01-084-1283) as reference.

Results and Discussion

Figure 1a shows XRD pattern of the as-synthesized TiO_2 samples. In the case of TiO_2 prepared by MW irradiation under lower φO_2 (MW-O5/MW-O10/MW-O20), two sets of diffraction peaks can be observed, corresponding to rutile TiO_2 and Ti_2O. With increasing of φO_2, the intensity of rutile diffraction peaks increased while Ti_2O peaks was disappeared, clearly demonstrates the progressive oxidation of target Ti. In addition, Figure 1b presents the change of lattice parameter of rutile TiO_2 as a function of φO_2. Interestingly, the lattice constant of a-axis and cell volume (V) significantly varied with φO_2, taking the minimum value in the sample MW-O10. In the case of sample synthesized at the lowest φO_2 (MW-O5), the a-axis lattice constant and V show the largest value. For samples synthesized under higher φO_2 (MW-O10, MW-O20, MW-O30), the a-axis lattice constant and V are much smaller than MW-O5 and these values are gradually increased as φO_2 increased. It has been reported that when oxygen vacancy is induced in TiO_2, the Ti-Ti and Ti-O bonds are strongly relaxed and the nearest-neighbor Ti atoms move outward from the vacancy along a-axial, leading to the expanding of lattice constant of a-axis[17]. Thus, the expended large a-axis constant and V in sample MW-O5 can be attributed to the induce of oxygen defects. On the other hand, in the case of TiO_2 possessing excessive oxygen atom, Ti-O bond is slightly relaxed because interstitial O atom repulse against lattice O atom, and coordinate with nearest-neighbor Ti atom, whose phenomenon seems to cause a slightly expanded lattice. It can be suggested that the TiO_2 prepared under higher φO_2 consists of both TiO_{2-x} and TiO_{2+y} states with regular arrangement of oxygen vacancy and excessive O atom, respectively.

Figure 2 shows Raman spectra of synthesized samples, summarized Raman shift of E_g mode of TiO_2 as a function of φO_2. As a result, characteristic peaks which are attributed Raman active modes of rutile crystal phase are observed in the spectra[18,19]. The peak of E_g mode is red-shifted with decrease of φO_2. The red-shifting of E_g can be attributed to the inducing of oxygen vacancy defects since it has been reported that E_g mode is sensitive against oxidation state of rutile TiO_2 in Raman spectra, which would be significantly red-shifted due to formation of oxygen vacancy defects in TiO_2[20,21].

The chemical structure of TiO_2 were furthermore investigated by confirming of surface chemical bonding sates via XPS, as shown in Figure 3. In the spectra of Ti_{2p} orbital (Figure 3a), the peaks varied from 458.8 to 458.9, 458.9, 458.6, and 458.3 eV with increasing of φO_2. These peaks are fitted by decomposed peaks at 458.8, 457.1 and 455.5 eV. The peak at 458.8 eV can be assigned as Ti^{4+} state in TiO_2, and the peaks at 457.1 and 455.5 eV
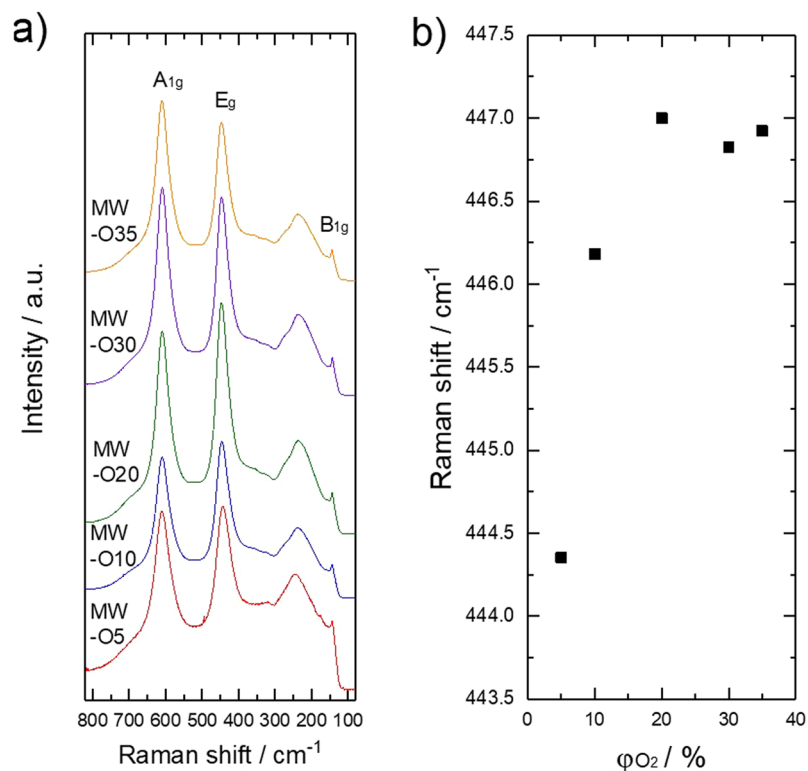
Figure 2. (**a**) Raman spectra of as-prepared TiO_2. (**b**) The Changes of the Raman shift of rutile TiO_2 Raman active modes (E_g mode).
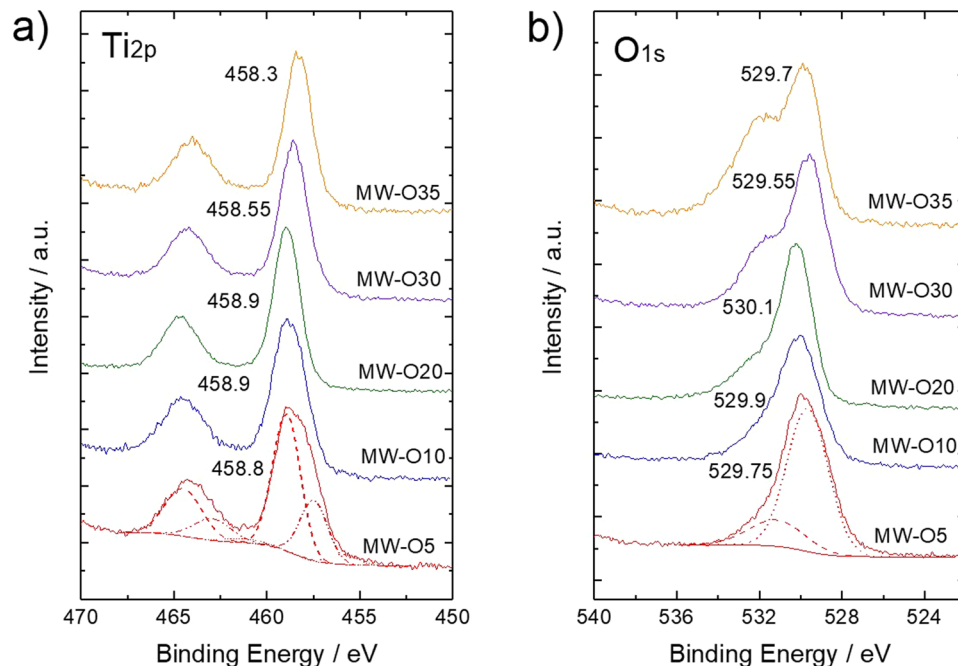
Figure 3. XPS spectra of core levels (**a**) Ti_{2p} and (**b**) O_{1s} related to as-prepared TiO_2. The number indicate the center value of peak top.

are assigned as Ti^{3+} and Ti^{2+}, whose binding energy is 1.7 and 3.4 eV lower than that of Ti^{4+}, respectively[22,23]. The peak components of Ti^{4+}, Ti^{3+} and Ti^{2+} as a function of φO_2 are summarized in Figure 4a. It can be clearly demonstrated that Ti^{3+} and Ti^{2+} components decrease as φO_2 decreases, while Ti^{4+} component increases as φO_2
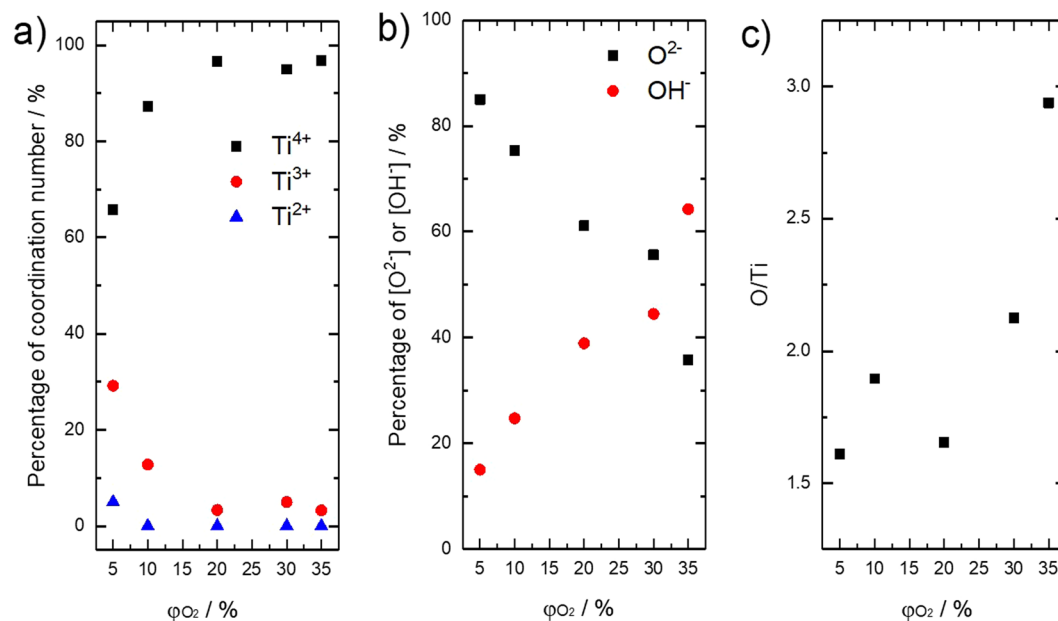
Figure 4. (**a**) Percentage of coordination number of titanium from XPS spectra of core levels Ti_{2p}. (**b**) Percentage of O^{2-} and OH^- from XPS spectra of core levels O_{1s}. (**c**) Composition of as-prepared TiO_2.

increases. As for O_{1s} spectra as shown in Figure 3b, peaks vary as 529.75, 529.9, 530.1, 529.55 and 529.7 eV for different samples and a shoulder peak appears at about 532.0 eV with φO_2 increases. These peaks at 530.1 and 531.7 eV are assigned as O^{2-} (Ti-O) and OH^-, respectively[23–25]. According to the results summarized in Figure 4b, the concentration of OH group increases with increase of φO_2. It has been reported that oxygen vacancy may induce dissociation of H_2O, then chemisorption of OH group takes place on the surface of TiO_2[1,26]. Thus, the obtained results indicate that the TiO_2 synthesized under high φO_2 contain high concentration of oxygen vacancy. Furthermore, this oxygen vacancy would induce strong relaxation between Ti-O bonding as being already described, leading to chemical shift of Ti^{4+} peak center in Ti_{2p} level toward lower binding energy. Figure 4c shows surface chemical composition of as-prepared samples estimated by peak area ratio in O_{1s} to Ti_{2p}. It demonstrates that excessive oxygen exists in TiO_2 lattice synthesized under high φO_2. Furthermore, the ratio of O/Ti was likely to decrease with decrease of φO_2. This result might be not consistent with the fact that TiO_2 synthesized under high φO_2 contains high concentration of oxygen vacancy. Thus, here we suggest that the obtained TiO_2 may possess quite specific chemical structure, which oxygen vacancy and interstitial oxygen atom coexist in TiO_2 crystal on top of particle surface.

The electrical absorption spectra of as-prepared sample were characterized as shown in Figure 5a. The as-prepared TiO_2 exhibit superior light absorption in visible region to compare with commercial rutile TiO_2. In addition, the shoulder peak from 400 to 500 nm gradually appear with increase of φO_2 due to formation of donor level between valence band (VB) and conduction band (CB) of TiO_2 caused by interstitial oxygen atom in lattice[27]. Furthermore, the optical bandgaps are calculated by Tauc plot in Figure 5b and the bandgap values are summarized as Figure 5c. As a result, the maximum value of bandgap is observed in sample MW-O20, whose value becomes significantly smaller with lower φO_2, while becomes slightly narrower with higher φO_2 as shown. As bandgap of sample MW-O10 gives value of 2.07 eV, it is in good agreement with TiO_2 where Ti^{3+} and oxygen vacancy introduce localized states at 0.75–1.18 eV below the CB minimum in the case of TiO_{2-x}[13]. On the other hand, although interstitial oxygen atom localized the state about 0.2~0.3 eV above the VB maximum in the existence of excessive oxygen in TiO_2 in general[27], the obtained bandgap of TiO_2 synthesized under high φO_2 (MW-O20, MW-O30 and MW-O35) were much narrower. According to the CCD photograph of synthesized TiO_2 as shown in Figure 6, the color of samples changed from metal gray to black, grey, ash grey and yellowish grey with different φO_2. It is known that TiO_{2+x} performs yellowish, on the contrast, the color of TiO_2 with oxygen vacancy become grey or black because trapped electron in oxygen vacancy act as color center. Thus, TiO_2 synthesized under high φO_2, especially MW-O20, MW-O30 and MW-O35 have complex impurity level caused by oxygen vacancy and interstitial oxygen atom, resulting in formation of narrow bandgap.

According to XRD pattern, Raman spectra and electrical absorption spectra results, it can be concluded that TiO_2 synthesized under high φO_2 exhibit specific TiO_{2+y}/TiO_{2-x}-TiO_{2+z} core/shell structure. Here, the formation mechanism of such core/shell TiO_2 during SMMW synthesis is concluded in Figure 7. We suggest that the specific heat history in MW heating is one of key points to form the above specific particle structure. During MW synthesis under high φO_2 system, TiO_{2+y} would be firstly formed at high temperature, and rapidly cooled to room temperature immediately after formation of TiO_2 due to lowering magnetic MW absorption, accompanying with large shrink of expanded lattice and introduction of high stress on outermost particle surface. Then the formed strain induces high concentration of defect, especially oxygen vacancy. It has been reported that rapid cooling after formation of oxide from metal target generates high concentration of defects on particle surface[28,29].
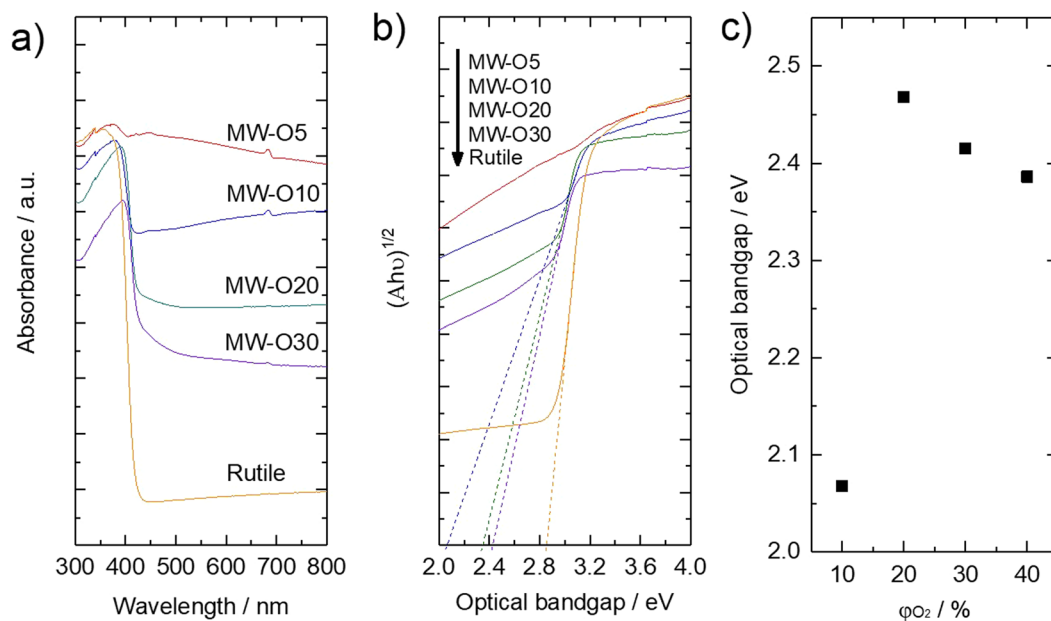
Figure 5. (**a**) UV-vis spectra of as-prepared TiO_2 and commercial rutile TiO_2. (**b**) Tauc plot. (**c**) Optical bandgap.

Furthermore, there are large densities of oxygen vacancies in TiO_2 which have plastic strain induced by two anvils[30]. Therefore, amorphous phase of TiO_{2-x}-TiO_{2+z} formed on TiO_{2+y}, resulting in formation of the specific core-shell structure. On the other hand, during MW synthesis under low φO_2 system, Ti^{3+} doped TiO_2 would be formed by the selective oxidation of Ti target in H-field throughout rapid heating and short reaction time[14].

We summarized the structure controlling mechanism for TiO_2 during SMMW reaction under different φO_2 as Figure 8. In the case of SMMW synthesis under low φO_2, Ti^{3+} self-doping TiO_2 is formed from Ti particle due to fast oxidation. TiO_2 synthesized under low φO_2 contains high Ti^{3+} concentration due to specific heat history through MW reaction. In this case, thermal non-equilibrium reaction lead to uncompleted oxidation of Ti and crystallization of TiO_2, resulting in formation of nonstoichiometric TiO_2. Under high φO_2, oxygen deficient TiO_2 could be formed by rapid cooling due to introduction of high stress on top surface though the formation of oxygen excessive TiO_2 at first. In the MW heating process, we control kind of introduced defect, Ti^{3+} and oxygen vacancy and specific chemical structure.

As an application of the prepared TiO_2 with well-controlled structure, the photocatalytic activity towards the degradation of RhB under visible irradiation was examined, whose results are summarized in Figure 9(a). The TiO_2 synthesized in low φO_2 (MW-10) exhibits excellent photocatalytic activity under visible light, which can be attributed to the increased light absorption as shown by Figure 5. It worth noting that our synthesized TiO_2, which possesses a mainly rutile phase and micro-ordered size show even better photocatalytic activity than the nano-ordered P25. The TiO_2 prepared under high low φO_2 (MW-20, MW-30) with specific core-shell structure show relative lower photocatalytic activity since high concentration of oxygen vacancies causes recombination of photo-excited carriers. In order to confirm the separation and recombination efficiency of photo-excited charge carriers, PL spectra is measured as Figure 9b. In general, the higher the recombination rate is, the stronger the PL peak intensity is[14,31]. As a result, the as-prepared TiO_2 exhibited lower recombination rate than commercial TiO_2, since the PL peak intensity decreases. In this case, the well separated electron and hole carriers transfer into the localized level of Ti^{3+} and VB respectively, leading to sufficient generation of $O_2\cdot$ and $OH\cdot$ radicals from the reduction of O_2 and oxidation reaction of H_2O[32–35]. Such active radicals finally contribute to photo-degradation of RhB under visible light. It can be expected that as-synthesized TiO_2 perform high photocatalytic efficiency than commercial TiO_2 with existence of sufficiently separated photo-excited carriers.

Conclusions

Structurally well-controlled TiO_2 are successfully synthesized via one-step SMMW assisted process under Ar and O_2 mixed atmosphere. Ti^{3+} self-doped TiO_2 and TiO_{2+y}/TiO_{2-x}-TiO_{2+z} core/shell TiO_2 are obtained by altering the volume fraction of O_2. The synthesized TiO_2 show sufficient light absorption in visible region and narrow band gap. In addition, superior photocatalytic activity for the photo-degradation of RhB under visible light irradiation is observed for the structure-controlled TiO_2. Despite a large particle size (micrometer order) and rutile crystal phase, our synthesized TiO_2 shows even better performance than commercial P-25 nanoparticle. The SMMW assisted synthesis process can provide new strategy for the preparation of functional metal oxides with well-controlled chemical structure and specific properties.
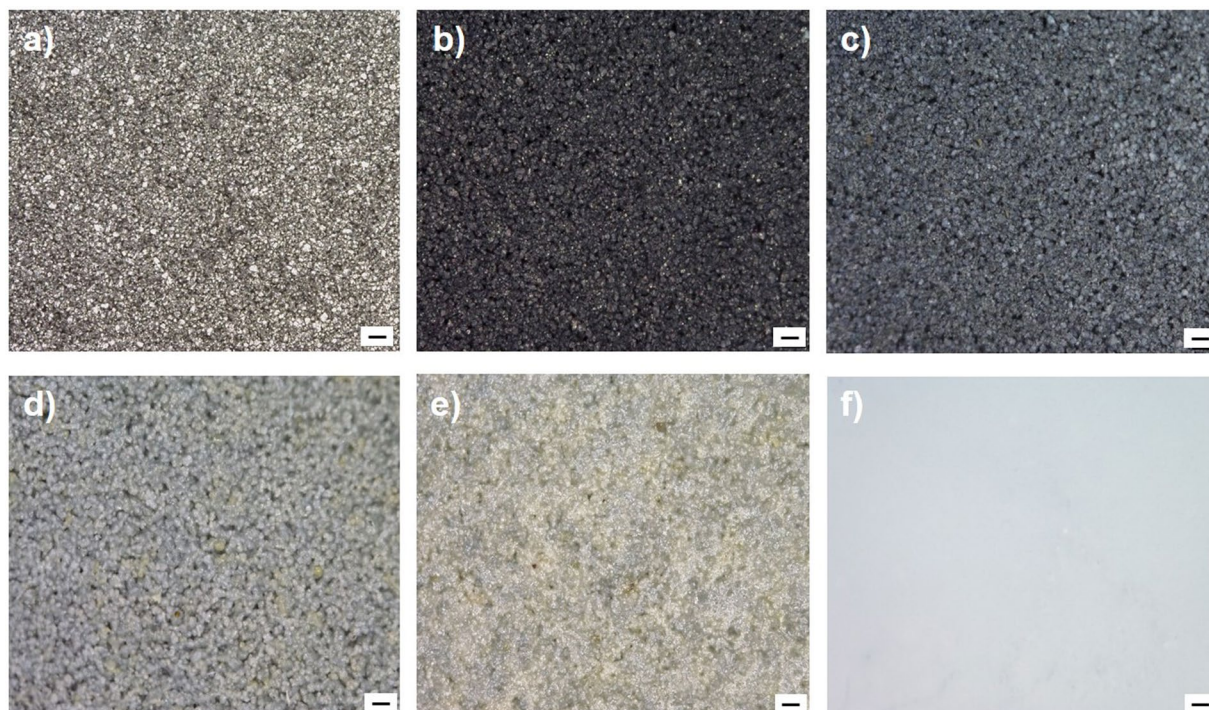
Figure 6. CCD images of raw Ti and as-prepared TiO2. (**a**) raw Ti, (**b**) MW-O5, (**c**) MW-O10, (**d**) MW-O20, (**e**) MW-O30, (**f**) P-25. The scale bar represents 100 μm.
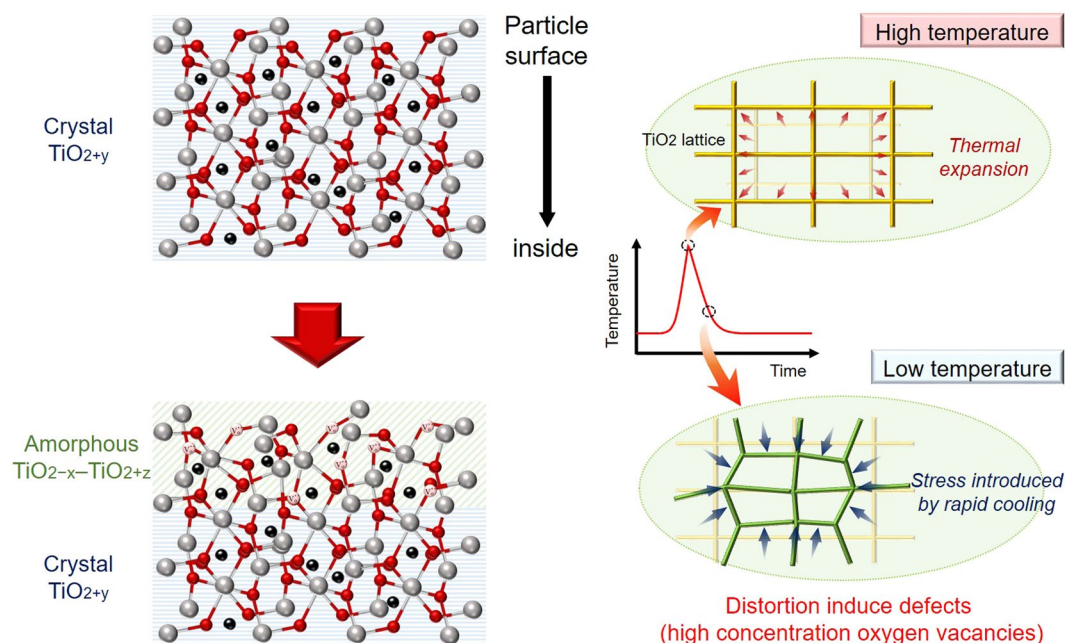

Figure 7. Mechanism of formation of TiO_{2+y} core/TiO_{2-x} – TiO_{2+z} shell structure in single-mode MW heating.

Methods

Materials and synthesis of TiOx. Titanium powder (3 N, powder under 45 μm mesh, Kojundo Chemical Laboratory, Japan) was used as raw material, and pelletized by uniaxial press. The pressure of 10 MPa was applied to a pellet of 10 mm in diameter. The TiO_2 were synthesized by magnetic MW heating using 2.45 GHz single-mode MW applicator for TE_{103} mode. The MW output was fixed at 100 W and Ti pellets were heated up under mixed atmosphere of argon and oxygen, whose volume fraction were controlled as $Ar/O_2 = 100$-x/x (x = 5, 10, 20 and 30, which named as MW-O5, MW-O10, MW-O20 and MW-O30, respectively).
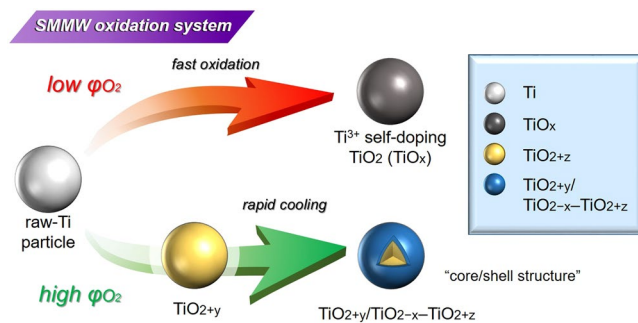
Figure 8. Mechanism of formation of nonstoichiometric TiO_2 by controlling atmosphere in MW heating.
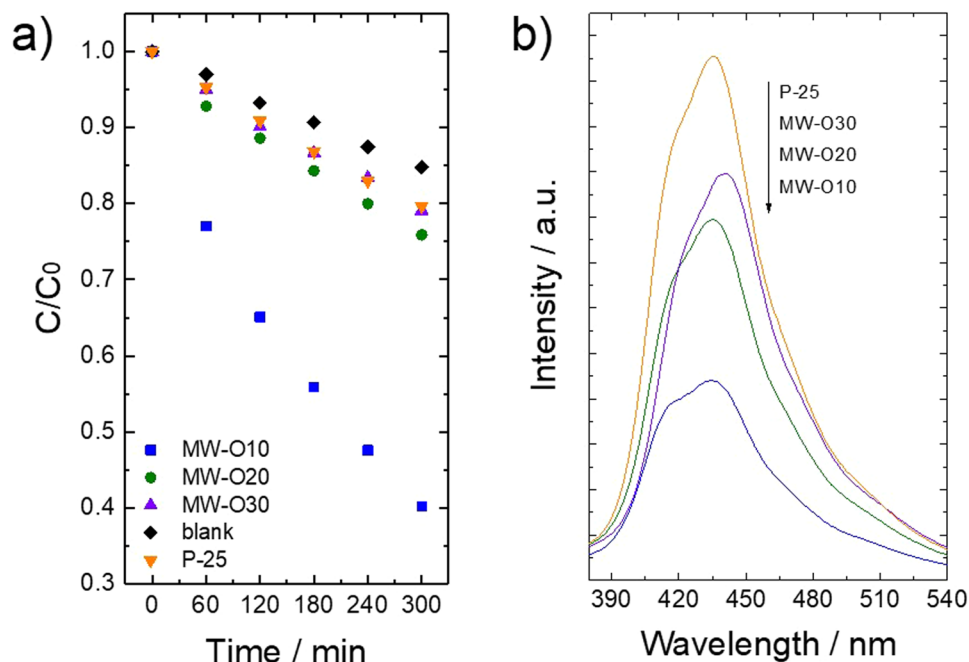
Figure 9. (**a**) Photocatalytic activity towards the degradation of Rhodamine B under irradiation of visible light for constant time (C/C_0 are the percentage photodegradation of RhB), (**b**) PL spectra of prepared TiO_2.

Characterization. The crystal structure of the raw material and as-prepared samples were analyzed by X-ray diffraction (XRD) measurement with Cu-Kα (Ultima IV, Rigaku, Japan). The crystal structure in particle surface of obtained sample was furtherly analyzed by Raman spectra (NRS-3100, Jasco, Japan) were measured. The surface chemical state was investigated by X-ray photoelectrical spectroscopy (XPS; M-prove, SSI, USA) with Al Kαsource (hν = 1486.6 eV). The shift of the binding energy due to relative surface charge-up was corrected using the Au_{4f} level at 83.98 eV and C_{1s} level at 284.8 eV. UV-vis absorbance spectra and photoluminescence (PL) spectra were measured by commercial UV-Vis spectrophotometer (V-7100, Jasco, Japan) and spectrofluorometer (FP-8500, Jasco, Japan) at an excitation wavelength of 350 nm, respectively.

Photocatalytic degradation of RhB. In photocatalytic experiments, as-prepared TiO_2 and commercial available TiO_2 pellets catalyst (P-25, Degussa) were loaded into 20 ml of RhB solution (5 ppm). A 200 W Hg-Xe lamp (LA-310UV, HAYASHI, Japan) and Xe lamp (LA-251Xe, HAYASHI, Japan) were used as UV and visible light source, whose powder density was settled as 1 mW cm^{-2}. Prior to irradiation, solutions with samples were left to stand in the dark for at least 180 min to ensure that the surface of photocatalysts were saturated with RhB. The RhB degradation was monitored by measuring the changes of UV-vis absorption spectra at 555 nm.

References

1. Hoffmann, M. R., Martin, S. T., Choi, W. & Bahnemann, D. W. Environmental applications of semiconductor photocatalysis. *Chem. Rev.* **95**, 69 (1995).
2. Fujishima, A., Tryk, D. A. & Rao, T. N. Titanium dioxide photocatalysis, *Photochem. Photobiol. C, Photochem. Rev.* **1**, 1 (2000).
3. Klosek, S. & Raftery, D. Visible Light Driven V-Doped TiO_2 Photocatalyst and Its Photooxidation of Ethanol. *J. Phys. Chem. B* **105**, 2815 (2001).

4. Iwasaki, M., Hara, M., Kawada, H., Tada, H. & Ito, S. Cobalt ion-doped TiO_2 photocatalyst response to visible light. *J. Colloid. Interf. Sci.* **224**, 202 (2000).
5. Ohno, T., Mitsui, T. & Matsumura, M. Photocatalytic Activity of S-doped TiO_2 Photocatalyst under Visible Light. *Chem. Lett.* **32**, 364 (2003).
6. Chen, X. & Burda, C. The Electronic Origin of the Visible-Light Absorption Properties of C-, N- and S-Doped TiO_2 Nanomaterials. *J. Am. Chem. Soc.* **130**, 5018 (2008).
7. Asahi, R., Morikawa, T., Ohwaki, T., Aoki, K. & Taga, Y. Visible-light photocatalysis in nitrogen-doped titanium oxides. *Science.* **293**, 269 (2001).
8. Irie, H., Watanabe, Y. & Hashimoto, K. Nitrogen-Concentration Dependence on Photocatalytic Activity of $TiO_{2-x}N_x$ Powders. *J. Phys. Chem. B* **107**, 5483 (2003).
9. Xing, M., Zhang, J., Chen, F. & Tian, B. An economic method to prepare vacuum activated photocatalysts with high photo-activities and photosensitivities. *Chem. Commun.* **47**, 4947 (2011).
10. Lu, G., Linsebigler, A. & Yates, J. T. Photocatalysis on TiO_2 surfaces: principles, mechanisms, and selected results. *J. Phys. Chem.* **98**, 11733 (1994).
11. Sasikala, R. *et al.* Highly dispersed phase of SnO_2 on TiO_2 nanoparticles synthesized by polyol-mediated route: Photocatalytic activity for hydrogen generation. *Int. J. Hydrogen Energy* **34**, 3621 (2009).
12. Zuo, F. *et al.* Self-Doped Ti^{3+} Enhanced Photocatalyst for Hydrogen Production under Visible Light. *J. Am. Chem. Soc.* **132**, 11856 (2010).
13. Nakamura, I. *et al.* Role of oxygen vacancy in the plasma-treated TiO_2 photocatalyst with visible light activity for NO removal. *J. Mol. Catal. A Chem.* **161**, 205 (2000).
14. Ozer, L. Y. *et al.* Long-Lasting Non-hydrogenated Dark Titanium Dioxide: Medium Vacuum Anneal for Enhanced Visible Activity of Modified Multiphase Photocatalysts. *ChemCatChem* **10**, 2949 (2018).
15. Kumar, S. G. & Koteswara Rao, K. S. R. Comparison of modification strategies towards enhanced charge carrier separation and photocatalytic degradation activity of metal oxide semiconductors (TiO_2, WO_3 and ZnO). *Appl. Surf. Sci.* **391**, 124 (2017).
16. Kato, K., Yunzi, X. & Shirai, T. A novel single-mode microwave assisted synthesis of metal oxide as visible-light photocatalyst. *materials letter* **235**, 125 (2019).
17. Santara, B., Giri, P. L., Imakita, K. & Fujii, M. Microscopic origin of lattice contraction and expansion in undoped rutile TiO_2 nanostructures. *J. Phys. D; Appl. Phys.* **47**, 215302 (2014).
18. Narayanan, P. S., Raman spectra of titanium dioxide, *Proc. Indian Acad. Sci. Sect. A* **32**, 279 (1950).
19. Lan, T., Tang, X. & Fultz, B. Phonon anharmonicity of rutile TiO_2 studied by Raman spectrometry and molecular dynamics simulations. *Phys. Rev. B.* **85**, 094305 (2012).
20. Parker, J. C. & Siegel, R. W. Raman microprobe study of nanophase TiO_2 and oxidation-induced spectral changes. *J. Mater. Res.* **5**, 1246 (1990).
21. Parker, J. C. & Siegel, R. W. Calibration of the Raman spectrum to the oxygen stoichiometry of nanophase TiO_2. *Appl. Phys. Lett.* **57**, 943 (1990).
22. Briggs, D. & Seah, M. P. Aurger and X-ray photoelectron spectroscopy, Practical Surface Analysis, (Wiley, New York, 1990).
23. Petigny, S. & Bourgeois, S. Superficial defects induced by argon and oxygen bombardments on (110) TiO_2. *surfaces, Surf. Sci.* **410**, 250 (1998).
24. Kumar, P. M., Badrinarayanan, S. & Sastry, M. Nanocrystalline TiO_2 studied by optical, FTIR and X-ray photoelectron spectroscopy: correlation to presence of surface states. *Thin Solid Films.* **358**, 122–130 (2000).
25. Erdem, B. *et al.* XPS and FTIR Surface Characterization of TiO2 Particles Used in Polymer Encapsulation. *Langmuir* **17**, 2664 (2001).
26. Schaub, R. *et al.* Oxygen Vacancies as Active Sites for Water Dissociation on Rutile TiO_2(110). *Phys. Rev. Lett.* **87**, 2661041 (2001).
27. Etacheri, V., Seery, M. K., Hinder, S. J. & Pillai, S. C. Oxygen rich titania: A dopant free, high temperature stable, and visible-light active anatase photocatalyst. *Adv. Funct. Mater.* **21**, 1 (2011).
28. Liang, C. H., Shimizu, Y., Sasaki, T. & Koshizaki, N. Preparation of ultrafine TiO_2 nanocrystals via pulsed-laser ablation of titanium metal in surfactant solution. *Appl. Phys. A* **80**, 819 (2005).
29. Niu, K. Y. *et al.* Morphology control of nanostructures via surface reaction of metal nanodroplets. *J. Am. Chem. Soc.* **132**, 9814 (2010).
30. Khosroshahi, H. R., Edalati, K., Arita, M., Horita, Z. & Fuji, M. Plastic strain and grain size effect on high-pressure phase transformations in nanostructured TiO_2 ceramics. *Scripta Materialia.* **124**, 59 (2016).
31. Li, F. B. & Li, X. Z. Photocatalytic properties of gold/gold ion-modified titanium dioxide for wastewater treatment. *Appl. Catal. A: General* **228**, 15 (2002).
32. Turchi, C. S. & Ollis, D. F. Photocatalytic degradation of organic water contaminants: Mechanisms involving hydroxyl radical attack. *Journal of Catalysis* **122**, 178 (1990).
33. Carter, E., Carley, A. F. & Murphy, D. M. Evidence for O_2^- radical stabilization at surface oxygen vacancies on polycrystalline TiO_2. *J. Phys. Chem. C* **111**, 10630 (2007).
34. Hirakawa, T., Yawata, K. & Nosaka, Y. Photocatalytic reactivity for O_2^- and OH radical formation in anatase and rutile TiO_2 suspension as the effect of H_2O_2 addition. *Appl. Catal. A* **325**, 105 (2007).
35. Cao, Y. Q. *et al.* TiO_xN_y modified TiO_2 powders prepared by plasma enhanced atomic layer deposition for highly visible light photocatalysis. *Scientific Reports* **8**, 12131 (2018).

Author Contributions

K. Kato planned the work, performed the experiments, characterized the results and wrote the manuscript. Y. Xin helps in the interpretation of characterization and writing manuscript. T. Shirai supervised the project, contributed to planning the work and provided the interpretation of characterization.

Additional Information